# Systems biology-enabled targeting of NF-κB and BCL2 overcomes microenvironment-mediated BH3-mimetic resistance in DLBCL.

Running title: Disentangling NF-κB and BCL2 in DLBCL

Aimilia Vareli[1], Haripriya Vaidehi Narayanan[2], Heather Clark[1], Eleanor Jayawant[1], Hui Zhou[3], Yi Liu[3], Lauren Stott[1], Fabio Simoes[1], Alexander Hoffmann[2], Andrea Pepper[1], Chris Pepper[1], Simon Mitchell[1†].

[1] Department of Clinical and Experimental Medicine, Brighton and Sussex Medical School, Falmer, United Kingdom; [1] Department of Clinical and Experimental Medicine, Brighton and Sussex Medical School, Falmer, United Kingdom; [2]Signaling Systems Laboratory, Department of Microbiology, Immunology, and Molecular Genetics, and Institute for Quantitative and Computational Biosciences, University of California, Los Angeles, Los Angeles, CA, United States; [3]DeepKinase Biotechnologies, Beijing, China

[†] S.A.Mitchell@bsms.ac.uk

Abstract: 198 words

Text: 3472 words

Figures: 8

References: 64

**Abstract**

In Diffuse Large B-cell Lymphoma (DLBCL), elevated anti-apoptotic BCL2-family proteins (e.g., MCL1, BCL2, BCLXL) and NF-κB subunits (RelA, RelB, cRel) confer poor prognosis. Heterogeneous expression, regulatory complexity, and redundancy offsetting the inhibition of individual proteins, complicate the assignment of targeted therapy. We combined flow cytometry 'fingerprinting', immunofluorescence imaging, and computational modeling to identify therapeutic vulnerabilities in DLBCL. The combined workflow predicted selective responses to BCL2 inhibition (venetoclax) and non-canonical NF-κB inhibition (Amgen16). Within the U2932 cell line we identified distinct resistance mechanisms to BCL2 inhibition in cellular sub-populations recapitulating intratumoral heterogeneity. Co-cultures with CD40L-expressing stromal cells, mimicking the tumor microenvironment (TME), induced resistance to BCL2 and BCLXL targeting BH3-mimetics via cell-type specific upregulation of BCLXL or MCL1. Computational models, validated experimentally, showed that basal NF-κB activation determined whether CD40 activation drove BH3-mimetic resistance through upregulation of RelB and BCLXL, or cRel and MCL1. High basal NF-κB activity could be overcome by inhibiting BTK to resensitize cells to BH3-mimetics in CD40L co-culture. Importantly, non-canonical NF-κB inhibition overcame heterogeneous compensatory BCL2 upregulation, restoring sensitivity to both BCL2- and BCLXL-targeting BH3-mimetics. Combined molecular fingerprinting and computational modelling provides a strategy for the precision use of BH3-mimetics and NF-κB inhibitors in DLBCL.

**Introduction**

Diffuse large B-cell lymphoma (DLBCL), is an aggressive blood cancer (1). First line treatment is only successful in approximately 60% of patients (2-5). The highly heterogenous nature of the disease has challenged advancing the standard of care through one-size-fits-all approaches (6-11). Activated B-cell (ABC) DLBCL patients bearing Nuclear Factor-κappa light chain enhancer of B cells (NF-κB)

activating mutations, and Germinal Center (GC) DLBCL patients with *BCL2*-activating mutations have particularly poor prognosis (11).

NF-κB is a dimeric transcription factor composed of combinations of five proteins (RelA, RelB, cRel, p50 and p52), which are normally sequestered in the cytoplasm by a combination of four inhibitors of NF-κB (IκBα, -β, -δ, and-ε) (12, 13). The IκB proteins have distinct affinities for different NF-κB dimers with IκBα predominantly inhibiting RelA-containing dimers and IκB-δ and -ε regulating cRel-containing dimers in a context-specific manner (14, 15). The abundance and nuclear localization of individual NF-κB components is prognostically informative in DLBCL (16-18). Heterogeneity in NF-κB subunits can be quantified and visualized using flow cytometry to reveal unique 'fingerprints' of NF-κB, with heterogenous levels of individual NF-κB proteins found within ABC-DLBCL (19). Two NF-κB pathways (canonical and non-canonical) may be activated by a combination of tumor microenvironmental signaling and activating mutations in DLBCL leading to nuclear translocation of NF-κB (20). While targeting NF-κB has shown therapeutic potential in subgroups of blood cancer patients (21-26), heterogeneity and toxicities associated with global targeting of the canonical NF-κB pathway has challenged clinical progress. The oncogenic role of NF-κB in lymphoma is largely attributed to the anti-apoptotic gene expression induced upon NF-κB activation (26, 27).

Anti-apoptotic BCL2 family proteins, including Myeloid Cell Leukemia 1 (MCL1) and B-cell Lymphoma-extra Large (BCLXL), are inhibitors of the intrinsic pathway of apoptosis (28, 29), and are often overexpressed in DLBCL as a result of gene translocation events, gene amplifications, mutations within open reading frames, and microenvironment-mediated increased NF-κB activity (30). BCL2 is an attractive target in DLBCL, and the specific BCL2 inhibitor venetoclax is clinically used for multiple hematological malignancies (31). However, venetoclax has shown limited efficacy in DLBCL clinical trials (31, 32). BCL2-family proteins (MCL1 and BCLXL) are often over expressed in DLBCL with elevated expression conferring venetoclax resistance by compensating for the

69 sequestration of BCL2 (33, 34). BH3-profiling, established in 2006, measured the impact of BH3-
70 peptides on mitochondrial outer membrane permeabilization (35). While predictive of response to
71 BCL2 antagonism in pre-clinical studies, responses to BH3-mimetics in drug response assays can
72 differ, and BH3-profiling has not translated into prospective assignment of therapies in clinical trials
73 of lymphoma (36-38).
74 The daunting complexity of both NF-κB regulatory networks, and apoptotic signaling regulation, has
75 motivated the use of computational systems biology models to predict responses to BH3-mimetics
76 (39), responses to the tumor microenvironment (TME) (19, 40), and predict the impact of mutations
77 on clinical outcome (19, 41). Recent single-cell RNA sequencing of DLBCL patient material revealed
78 the primary impact of the TME is through CD40 and B-cell activating factor (BAFF), which activate
79 non-canonical NF-κB (25). The regulation of BCLXL by non-canonical NF-κB (RelB) is established in
80 CLL (25). However, how heterogeneity in multiple NF-κB proteins results in anti-apoptotic protein
81 heterogeneity in the context of the TME, and controls response to BH3-mimetics is unknown and has
82 the potential unlock the deployment of targeted therapies such as BH3-mimetics and NF-κB
83 inhibitors (Figure 1).

84 **Methods**

85 **Mice**

86 Primary B cells were acquired from C57BL/6 WT/IκBε$^{-/-}$/IκBα$^{mut}$ female mice (9-12 weeks old),
87 spleens were homogenized and splenocytes were stained with anti-CD43, prior to purification by
88 negative column selection (Miltenyi Biotec, Cologne Germany) as described (14, 42). B cell purity
89 was assessed by flow cytometry staining for anti-B220. Mice were maintained in environmental
90 control facilities at the University of California, Los Angeles. Animal work was performed according
91 to University of California, Los Angeles regulations, under an approved protocol.

92 **Cell culture**

93 DLBCL cell lines were sourced from DSMZ (Braunschweig, Germany) and cultured in recommended
94 medium. Cells were kept at 37°C in 5% $CO_2$ conditions and routinely tested for mycoplasma
95 contamination. NIH3T3 cells transfected to stably express human CD40 (hCD40L-3T3) were
96 obtained from Prof Chris Pepper (Brighton and Sussex Medical School, UK) and transfection was
97 maintained by puromycin selection (0.1%).

98 **Co-culture**

99 DLBCL cells were co-cultured with hCD40L-3T3, or non-transfected control cells for 24 hours on 96-
100 well flat bottom plates, with or without small molecule inhibitors.

101 **Drug Treatments**

102 $0.1 \times 10^5$ DLBCL cells were plated per well and treated with Amgen16 used at concentrations of 1.25-
103 100μM purchased from Merck (Gillingham, UK). ABT199 (venetoclax) was purchased from
104 Selleckchem (Texas, USA) and used at concentrations of 0.0001-100μM with or without Amgen16 at
105 a dose of 50μM for 24 hours.

106 **Flow Cytometry**

107 Early apoptosis was determined by flow cytometry following Annexin V staining (BioLegend) and data
108 was acquired on a CytoFlex LX, using the BD fix and perm kit (BioLegend), and data was acquired as
109 previously described (19).

110 **Proteomics**

111 Equal amounts of protein determined using BCA assay, from each sample were digested using
112 trypsin. For tyrosine phosphoproteomics, peptides were enriched using SH2-superbinder beads as
113 described (43), and the flow-through reconstituted in freshly prepared sample loading buffer and
114 subjected to phosphopeptide enrichment using $TiO_2$ beads preconditioned with the loading buffer
115 for 5 minutes. Data-independent acquisition mass spectrometry (DIA-MS) experiments were
116 performed on a ThermoFisher Orbitrap Astral mass spectrometer. A DIA spectral library generated

using DIA-MS2pep was utilized in DIA-NN software for protein quantification, with precursor and protein false discovery rates (FDR) set to 1%. Heatmaps were generated using R package pheatmap (version 1.0.12).

**Immunofluorescent Microscopy**

NF-κB activity was determined post fixation with 4% PFA and permeabilization with 0.1% Triton-X. Cells were stained with anti-p65 (Invitrogen), RelB (Cell signaling), cRel (Invitrogen), DAPI (ThermoFisher) and rhodamine phalloidin (Thermo Scientific). Images were captured with *Operetta CLS*, and nuclear:cytoplasmic ratios of NF-κB proteins were analyzed with *Cell Profiler*.

**Simulations**

The computational model and simulation method is described previously (40). Basal canonical pathway activation was increasing 0% to 0.5%. NIK degradation was decreased using the equation *NIK deg=1/(1+(t/600))*. 25 individual simulations were run for each cell line with parameter sampling as described previously (40, 44). Models were solved using the Julia DifferentialEquations.jl package (45).

**Statistical Analysis**

All statistical analysis was performed using GraphPad Prism 10.0 (California, USA) and Julia 1.8.5. Analysis of paired datasets was performed with paired t-tests, whereas unpaired t-tests and one-way ANOVA to analyze differences between groups, followed by indicated post-hoc tests. $LC_{50}$ values were generated a post four-parameter linear regression test. Flow cytometry data was analyzed on CytExpert Software (Beckman Coulter). $*P<0.5$; $**P<0.01$; $***P<0.001$; $****P<0.0001$.

**Results**

**Flow cytometry-based 'fingerprinting' predicts sensitivity to inhibitors targeting non-canonical NF-κB and BCL2**

141 Previous work in which NF-κB subunit abundance was visualized as contoured density plots standardized
142 using z-scores (Figure 2A) established heterogeneity in RelA abundance between ABC-DLCBL cell lines
143 (19). To establish whether similar variability is present in ABC- and GC-DLBCL we measured the levels of
144 NF-κB in two ABC- (RIVA and U2932) and two GC-DLBCL (SUDHL8 and SUDHL10) cell lines (Figure 2B),
145 and identified varied expression of both RelA and RelB, which did not align with COO (Figure 2B). While
146 there was no variability in RelB between ABC cell lines (RIVA and U2932, Figure 2C), as reported previously
147 (19), GC-DLBCL cell line SUDHL10 was found to have significantly higher RelB (Figure 2B and C) and a
148 higher ratio of RelB to RelA (Figure 2B). We hypothesized that this cell line may be sensitive to NIK
149 inhibition, and found NIK-inhibitor Amgen16 was significantly more effective at killing SUDHL10 cells than
150 cell lines with lower levels of RelB (Figure 2D and E, $p<0.01$).
151 We next sought to establish whether a similar approach could enable predictable targeting of BCL2-family
152 proteins. We identified two lines with low BCL2 (SUDHL8, and SUDHL10, Figure 2F), and two lines with
153 significantly higher BCL2 (U2932, and RIVA, Figure 2G, $p<0.0001$). In agreement with clinical observations
154 (31), we found that ABT199 had significantly higher efficacy in cell lines with high BCL2 (21H and I, $p<0.01$).
155 Previous BH3-profiling had suggested a complete block of apoptosis in SUDHL10 cells due to loss of
156 effector proteins (Bak/Bax) (36); however, multiple recent studies have found substantial Bax
157 expression in SUDHL10 cells, and implicated low BCL2 expression in resistance to venetoclax in
158 SUDHL10 cells (34, 46). NF-κB profiling (Figure 2B) revealed a vulnerability to NIK inhibition (Figure 2D-
159 E), indicating the potential for combined NF-κB and BCL2 "fingerprinting'' to inform the rational
160 assignment of therapeutic agents targeting multiple pathways in DLBCL.
161
162 **BCL2 family protein heterogeneity confers heterogenous responses to ABT199 within a biclonal**
163 **DLBCL cell line**
164 The U2932 cell line harbors two phenotypically and genetically distinct subclones. The subclone R1
165 is CD20, CD38 high, while the R2 subclone is CD20, CD38 low (19, 47). We found that the R1

166 subclone (Figure 3A) was ABT199 resistant, whereas the R2 subclone was ABT199 sensitive, even at
167 the lowest dose of ABT199 tested (0.0001μM) (Figure 3B). While BCL2 protein abundances could not
168 explain the different sensitivities to ABT199 (Figure 3C), we identified significantly higher MCL1 in
169 the R1 subclone (Figure 3C, $p<0.0001$). To determine if the selective sensitivity of the R2 subclone to
170 ABT199 would be retained when DLBCL cells are activated by their TME we employed a co-culture
171 system of hCD40L-3T3, which multiple studies have shown mimics both cell-contact and the
172 presence of activated T cells in the DLBCL TME (24, 33, 34, 48)(Figure 3D). The R2 subclone became
173 substantially more resistant in the co-culture system (Figure 3E), significantly increasing resistance
174 to ABT199 (Figure 3F, $p<0.01$). In hCD40L-3T3 BCLXL was significantly more induced than both BCL2
175 ($p<0.05$) and MCL1 ($p<0.01$) which were either unchanged (BCL2) or moderately decreased (MCL1)
176 (Figure 3G). Within the U2932 cell lines we identified multiple distinct resistance mechanisms to
177 ABT199; high MCL1 in the R1 subclone, and high BCLXL in the context of CD40L co-culture.

178 **TME-mediated resistance to BH3-mimetics can result from induction of multiple compensatory**
179 **BCL2-family proteins**

180 Repeating analysis in the BCL2-dependent RIVA cells identified significant TME-mediated ABT199
181 resistance in hCD40L-3T3 co-culture (Figure 4A and B, $p<0.05$) and a significant increase in BCLXL
182 (Figure 4C, $p<0.01$). This effect was dependent on CD40L as untransfected NIH3T3s did not
183 upregulate BCLXL (supplemental Figure 1,2 and 4).

184 To establish whether this effect was unique to venetoclax we employed the SUDHL8 cell line, which
185 has established sensitivity to BCLXL inhibition by the BH3- mimetic A1331852 (34). SUDHL8 cells
186 were significantly resistant to BCLXL inhibition in hCD40L-3T3 co-culture (Figure 4D-E, $p<0.001$).
187 Significantly more MCL1 was induced than either BCLXL or BCL2 in hCD40L-3T3 co-culture (Figure
188 4F, $p<0.05$). This effect was not seen in co-culture with untransfected NIH3T3s (supplemental Figure
189 3 and 4). While CD40 is known to activate non-canonical NF-κB signaling component RelB, which

190 has been shown to control BCLXL expression in related hematological malignancies (25), the control
191 of MCL1 by specific NF-κB subunits is less clear, particular in the context of lymphoma (Figure 1A).

192 **The SUDHL8 cell line has high basal nuclear NF-κB RelA activity through elevated B cell receptor**
193 **signaling.**

194 We hypothesized that the canonical RelA- or cRel-containing NF-κB dimers could be responsible for
195 cell line-specific induction of BH3-mimetic resistance through MCL1 (Figure 5A). Quantification of
196 the nuclear activity of NF-κB RelA and cRel using immunofluorescence microscopy (Figure 5B,
197 Supplemental Figure 5) revealed substantial cell-to-cell variability in nuclear NF-κB activity (Figure
198 5C), and significantly higher nuclear RelA in the SUDHL8 cell line (Figure 5D, bottom).

199 We performed global, and serine threonine proteomics in the cell line with elevated nuclear RelA
200 (SUDHL8), a line with low nuclear RelA (U2932), and a line dependent on non-canonical signaling
201 (SUDHL10), to test whether elevated B Cell Receptor (BCR) signaling was responsible for elevated
202 nuclear RelA. These data show substantially elevated CD19 and SYK abundance and
203 phosphorylation levels in SUDHL8 compared to U2932 and SUDHL10 (supplemental Figure 6A-B).
204 BTK abundance in SUDHL8 was not elevated; however, phosphorylated Y223 in the BTK SH3 domain
205 has recently been found to mirror catalytic activity (49). Phosphotyrosine (pY) proteomics revealed
206 elevated phosphorylation at BTK_Y223 in SUDHL8 cells (1.8 fold) consistent with elevated BTK
207 activity (supplemental Figure 6C).

208 As CD40L is a selective activator of non-canonical NF-κB signaling in B cells (50), it is not clear how
209 elevated BTK activity and RelA nuclear abundance in SUDHL8 could confer CD40-mediated
210 induction of MCL1 (Figure 5A). IκBα, IκBε, and p100/IκBδ are all induced by RelA activity (12), and are
211 preferential inhibitors of distinct NF-κB subunits (Figure 5A)(14, 40, 42). Therefore, we hypothesized
212 that the altered profile of NF-κB inhibitors could control distinct responses to the TME, and sought to
213 establish how this could lead to selective induction of MCL1.

214 **Computational modelling informed by imaging experiments predicts that high basal nuclear**
215 **NF-κB RelA leads to crosstalk, with CD40-mediatead induction of cRel**

216 Employing established computational models of NF-κB signaling (19, 40), and running two
217 simulations differing only in the degree to which basal BCR-signaling was elevated, predicted that
218 RelA:p50 is mainly inhibited by IκBα in RIVA cells (Figure 6A). SUDHL8 cells were predicted to have
219 reduced inhibition of RelA and a moderate shift in inhibitor composition (away from IκBα and IκBε,
220 Figure 6A–left). The predicted impact of high basal canonical pathway activation on cRel:p50 was
221 markedly different (Figure 6A, right), shifting towards IκBδ inhibition of cRel in SUDHL8 cells, with
222 <10% of cRel being inhibited by IκBα and -ε (Figure 6A right).

223 The steady state of these simulations (Figure 6B, t=0) recapitulated the selectively elevated nuclear
224 RelA, seen in immunofluorescence imaging (Figure 5D). Simulating co-culture mediated non-
225 canonical pathway activation revealed induction of RelB:p52, without induction of RelA:p50 (Figure
226 6B, left and center). However, induction of nuclear cRel:p50 was predicted only in the SUDHL8 cell
227 line (Figure 6B, right). Cells with low basal nuclear RelA, such as RIVA cells, reliably induce p100
228 processing to p52, and subsequent translocation of RelB:p52 to the nucleus upon CD40L activation
229 (Figure 6C). Simulations predict that constitutive activation of the BCR pathway results in
230 degradation of IκBα and IκBε, nuclear translocation of RelA:p50 and subsequent induction of p100,
231 which forms higher inhibitory complexes termed IκBδ (13). IκBδ has higher affinity for cRel than RelA
232 (14), resulting in sequestration of cRel by IκBδ prior to CD40L activation (Figure 6D, left). Upon CD40L
233 activation p100 is processed into a self-inhibited p100:p52 dimer, which frees cRel for nuclear
234 translocation (13, 42) (Figure 6D, right). This crosstalk mechanism was first identified in fibroblasts
235 (13), and shown to preferentially upregulate cRel in proliferating healthy B cells responding to BAFF
236 (42). This predicted crosstalk from non-canonical signaling to NF-κB cRel has not previously been

237 described in lymphoma or linked to induction of anti-apoptotic proteins, therefore we sought to
238 validate these computational predictions.
239
240 **Experimental validation of modelling predictions confirms crosstalk between CD40 and cRel**
241 **confers BH3-mimetic resistance and can be overcome with BTK inhibition**
242 Immunofluorescence imaging confirmed that hCD40L co-culture did not induce RelA (Figure 6E-F,
243 compare to 6B left), but did induce significantly higher levels of nuclear:cytoplasmic RelB in both the
244 RIVA and SUDHL8 cell lines, as predicted by computational simulations (Figure 6E-F, compared to
245 6B middle, $p<0.05$). Only in SUDHL8 cells was this accompanied by significantly increased nuclear
246 cRel, as predicted computationally (Figure 6E-F, compared to 6B right, $p<0.01$). hCD40L co-culture
247 with the addition of ibrutinib (targeting BTK) re-sensitized SUDHL8 cells to BCLXL inhibition,
248 confirming BCR-pathway activation was responsible for BH3-mimetic resistance in the SUDHL8
249 cells (Figure 6G-H, $p<0.001$).
250
251 **NF-κB cRel activity selectively induces MCL1 in B cells**
252 We hypothesized that crosstalk-mediated induction of cRel was responsible for the induction of
253 MCL1 (Figure 4F). ChIP-seq data generated in a lymphoblastoid B cell line (GM12878)(51), showed
254 promiscuous binding of all NF-κB subunits around the transcription start site (TSS) of *BCL2L1*
255 (encoding BCLXL), and no definitive binding of NF-κB subunits at the TSS for *BCL2*. The same data
256 revealed marginally higher levels of cRel binding than both RelB and RelA at the *MCL1* TSS (Figure
257 7A). To explore whether this was unique to the lymphoblastoid cell lines we collected Model-based
258 Analysis for ChIP-Seq 2 (MACS2) scores for NF-κB cRel, RelA and RelB within 1kb of the MCL1 TSS
259 across ChIP-Seq datasets reported in a ChIP-seq database (ChIP-Atlas (52), Figure 7B) confirmed
260 significantly higher binding of cRel than both RelA and RelB (Figure 7B, $p<0.0001$).

261 We sought an alternative method to selectively increase cRel activity in B cells. Computational
262 modelling of NF-κB in wild type (WT) B cells, IκBε knock-out B cells, and B cells bearing an IκBα
263 promoter mutation that lowered IκBα expression (IκBα$^{κB/κB}$), predicted that IκBε$^{-/-}$ induces cRel activity
264 significantly more than RelA activity (Figure 7D, $p<0.001$), while IκBα$^{κB/κB}$ would be non-selective
265 (Figure 7D). This was experimentally validated using data from IκBε$^{-/-}$ mouse B cells (Alves *et al.* 2014,
266 Figure 7D-E). Primary splenic B cells from IκBε$^{-/-}$ mice (Figure 7F, 95-99% purity, supplemental Figure
267 7) had significant selective induction of Mcl1 (Figure 7G, $p<0.05$), while IκBα$^{κB/κB}$ mice did not (Figure
268 7G). Together, this ChIP-seq analysis, computational modeling, and validation in primary mouse
269 models (Figure 7D-G) implicate cRel in the upregulation of MCL1 in DLBCL.
270

271 **Inhibition of the NF-κB inducing kinase (NIK) overcomes tumor microenvironment (TME)-**
272 **mediated BH3-mimetic resistance in DLBCL**

273 We sought to identify a single pharmacological intervention that could overcome the multiple
274 methods of TME-mediated resistance to multiple BH3-mimetics identified here. NIK inhibition using
275 Amgen16 (Figure 8A-B) achieved significant re-sensitization of the SUDHL8 cell lines to BCLXL
276 inhibition in hCD40L-3T3 co-culture (Figure 8C, $p<0.001$). Both cell lines that were ABT199 sensitive
277 in monoculture (U2932 and RIVA), and resistant in hCD40L-3T3 co-culture, were significantly re-
278 sensitized to ABT199 through treatment with the NIK inhibitor (Figure 8E and E, $p<0.05$).
279

280 **Discussion**

281 The molecular heterogeneity that characterizes DLBCL contributes to clinical resistance and relapse
282 (53, 54). While there is substantial evidence that aberrant NF-κB activation within the lymph node
283 TME, confers worse prognosis in DLBCL, the pharmacological targeting of this interaction has been
284 challenging due to toxicities associated with targeting the canonical NF-κB pathway (55). The present

285 study indicates that flow cytometry fingerprinting may enable identification and assignment of NIK-
286 inhibitors particularly in the recently identified subset of DLBCL with high RelB and poor prognosis (56).
287 BCL2 fingerprints confirmed that basal high basal BCL2 levels predicted sensitivity to ABT199, in
288 accordance with results from clinical trials (57, 58). When compared to other biochemical or
289 functional measurements such as BH3-profiling flow cytometry-based fingerprinting enables
290 identification of cellular sub populations within a heterogeneous tumor. We found that even within a
291 single cell line we could identify multiple venetoclax resistance mechanisms, including inherent
292 resistance due to high MCL1, and resistance acquired in the context of a TME-mimicking co-culture
293 through upregulation of BCLXL.
294 BCL2-targeting therapies create impressive responses in CLL, where the bulk of the disease is
295 circulating in the peripheral blood, however lymph-node mediated treatment resistance has been
296 implicated in the inability to cure CLL (59). In DLBCL, where the bulk of the disease is supported by
297 the lymph node TME, BCL2-targeting therapies have been far less effective. Increased non-canonical
298 NF-κB activity, and BCLXL, may provide a rationale for the lack of efficacy of ABT199 in DLBCL. NIK
299 inhibition was effective in all cell lines tested here: either as a monotherapy in RelB high DLBCL
300 (Figure 2B), to re-sensitize BCL2-sensitive DLBCL to ABT199 in the TME (Figure 8D and E), or to re-
301 sensitize BCLXL-sensitive DLBCL to BCLXL targeting BH3-mimetics in the TME (Figure 8C). This
302 finding is supported by studies in CLL (24, 25).
303 We discovered unexpected induction of MCL1 in cells with elevated basal NF-κB activity.
304 Incorporating NF-κB activity information into computational models led to a prediction of signaling
305 crosstalk between the two NF-κB pathways, which was experimentally confirmed. Our data
306 implicate cRel as a regulator of MCL1 in DLBCL, which was previously unknown (60). cRel-mediated
307 gene expression has been correlated with GC-DLBCL (61), and pre-clinical MCL1 inhibitors show
308 increased efficacy in GC-DLBCL (62). As MCL1 inhibitors are currently reaching first-in-human

309 studies (63), a predictive understanding of how the TME controls abundance of anti-apoptotic
310 proteins through NF-κB will be key to successful trial design and clinical adoption. This study
311 highlights the importance of understanding the impact of TME-mediated signaling, which may not be
312 captured in assays performed on isolated cells or isolated mitochondria (64).
313 Computational simulations can: predict DLBCL responses to BH3-mimetics (39), integrate flow
314 cytometry and mutational information to predict DLBCL signaling responses to the TME (19), and
315 predict unexpected crosstalk between the TME and anti-apoptotic proteins. Integration of high
316 dimensional data with computational modelling enables assignment of targeted therapies that can
317 overcome the protective effect of the TME. While detailed molecular characterization is unlikely to
318 be incorporated into the standard of care for all DLBCL patients, computational simulations
319 informed by genetic profiling of diagnostic samples enable the identification of DLBCL patients that
320 are molecularly predisposed to a poor response (41). Such a prediction motivates further combined
321 molecular profiling and computational modeling in order to assign efficacious targeted therapeutic
322 approaches to the subset patients who will not respond to the standard of care.

**Acknowledgments**

We would like to thank all members of the Mitchell and Pepper labs for valuable discussions. This study was supported by *Leukaemia UK John Goldman Fellowship 2020/JGF/003, UKRI Future Leaders Fellowship (MR/T041889/1) and Paul Stanforth PhD Studentship* (to S.M), *Blood Cancer UK 23004* (to C.P), *MRC MR/V009095/1* (to A.P), *NIH R01AI132731 and R01AI127867* (to A.H).

**Data Availability Statement**

The computational code and analysis pipelines generated during and/or analyzed during the current study are available in the GitHub repository, https://github.com/SiFTW/VareliEtAl/. Any other data generated during and/or analyzed during the current study are available from the corresponding author on reasonable request.

**Authorship Contributions**

Contribution: **A.V** designed the research, performed experiments, analyzed data, designed figures and wrote the manuscript; **H.V.N** performed experiments, cosupervised part of the study and reviewed the manuscript; **H.C, E.J, L.S** performed experiments; **H.Z., Y.L** performed experiments, analyzed data, designed figures and wrote the manuscript; **F.S** interpreted data and reviewed the manuscript; **A.H** contributed vital new reagents, interpreted data, supervised part of the study and reviewed the manuscript; **A.P, C.P** designed the research, cosupervised the study and reviewed the manuscript; **S.M** designed the research, supervised the study, performed experiments, analyzed data, designed figures and wrote the manuscript.

**Disclosure of Conflicts of Interest:** Yi Liu is a shareholder of DeepKinase Biotechnologies.

343 **References**


344 1. Davies A, Barrans S, Burton C, Mercer K, Caddy J, Chinnery F, et al. ACCEPT - combining
345 acalabrutinib with rituximab, cyclophosphamide, doxorubicin, vincristine and prednisolone (R-
346 CHOP) for Diffuse Large B-cell Lymphoma (DLBCL): study protocol for a Phase Ib/II open-label
347 non-randomised clinical trial. F1000Res. 2020;9:941.
348 2. Meng F, Zhong D, Zhang L, Shao Y, Ma Q. Efficacy and safety of rituximab combined with
349 chemotherapy in the treatment of diffuse large B-cell lymphoma: a meta-analysis. Int J Clin Exp
350 Med. 2015;8(10):17515-22.
351 3. Feugier P, Hoof AV, Sebban C, Solal-Celigny P, Bouabdallah R, Fermé C, et al. Long-
352 Term Results of the R-CHOP Study in the Treatment of Elderly Patients With Diffuse Large B-
353 Cell Lymphoma: A Study by the Groupe d'Etude des Lymphomes de l'Adulte. Journal of Clinical
354 Oncology. 2005;23(18):4117-26.
355 4. Tilly H, Morschhauser F, Sehn LH, Friedberg JW, Trněný M, Sharman JP, et al.
356 Polatuzumab vedotin in previously untreated diffuse large B-cell lymphoma. New England Journal
357 of Medicine. 2022;386(4):351-63.
358 5. Bartlett NL, Wilson WH, Jung S-H, Hsi ED, Maurer MJ, Pederson LD, et al. Dose-adjusted
359 EPOCH-R compared with R-CHOP as frontline therapy for diffuse large B-cell lymphoma: clinical
360 outcomes of the phase III intergroup trial alliance/CALGB 50303. Journal of clinical oncology.
361 2019;37(21):1790-9.
362 6. Hunter E, McCord R, Ramadass AS, Green J, Westra JW, Mundt K, et al. Comparative
363 molecular cell-of-origin classification of diffuse large B-cell lymphoma based on liquid and tissue
364 biopsies. Translational Medicine Communications. 2020;5(1):5.
365 7. Swerdlow SH, Campo E, Pileri SA, Harris NL, Stein H, Siebert R, et al. The 2016 revision
366 of the World Health Organization classification of lymphoid neoplasms. Blood.
367 2016;127(20):2375-90.
368 8. Vaidya R, Witzig TE. Prognostic factors for diffuse large B-cell lymphoma in the
369 R(X)CHOP era. Ann Oncol. 2014;25(11):2124-33.
370 9. Priebe V, Sartori G, Napoli S, Chung EYL, Cascione L, Kwee I, et al. Role of ETS1 in the
371 Transcriptional Network of Diffuse Large B Cell Lymphoma of the Activated B Cell-Like Type.
372 Cancers. 2020;12(7):1912.
373 10. Pasqualucci L, Dalla-Favera R. Genetics of diffuse large B-cell lymphoma. Blood.
374 2018;131(21):2307-19.
375 11. Chapuy B, Stewart C, Dunford AJ, Kim J, Kamburov A, Redd RA, et al. Molecular subtypes
376 of diffuse large B cell lymphoma are associated with distinct pathogenic mechanisms and
377 outcomes. Nature Medicine. 2018;24(5):679-90.
378 12. Mitchell S, Vargas J, Hoffmann A. Signaling via the NFκB system. WIREs Systems
379 Biology and Medicine. 2016;8(3):227-41.
380 13. Basak S, Kim H, Kearns JD, Tergaonkar V, O'Dea E, Werner SL, et al. A fourth IκB protein
381 within the NF-κB signaling module. Cell. 2007;128(2):369-81.
382 14. Alves BN, Tsui R, Almaden J, Shokhirev MN, Davis-Turak J, Fujimoto J, et al. IκBε is a
383 key regulator of B cell expansion by providing negative feedback on cRel and RelA in a stimulus-
384 specific manner. The Journal of Immunology. 2014;192(7):3121-32.
385 15. Almaden JV, Tsui R, Liu YC, Birnbaum H, Shokhirev MN, Ngo KA, et al. A pathway switch
386 directs BAFF signaling to distinct NFκB transcription factors in maturing and proliferating B cells.
387 Cell reports. 2014;9(6):2098-111.

16. Davis RE, Brown KD, Siebenlist U, Staudt LM. Constitutive nuclear factor κB activity is required for survival of activated B cell–like diffuse large B cell lymphoma cells. The Journal of experimental medicine. 2001;194(12):1861-74.
17. Curry CV, Ewton AA, Olsen RJ, Logan BR, Preti HA, Liu Y-C, et al. Prognostic impact of C-REL expression in diffuse large B-cell lymphoma. Journal of hematopathology. 2009;2:20-6.
18. Eluard B, Nuan-Aliman S, Faumont N, Collares D, Bordereaux D, Montagne A, et al. The alternative RelB NF-κB subunit is a novel critical player in diffuse large B-cell lymphoma. Blood, The Journal of the American Society of Hematology. 2022;139(3):384-98.
19. Jayawant E, Pack A, Clark H, Kennedy E, Ghodke A, Jones J, et al. NF-κB fingerprinting reveals heterogeneous NF-κB composition in diffuse large B-cell lymphoma. Frontiers in Oncology. 2023;13.
20. Pasqualucci L, Klein U. NF-κB mutations in germinal center B-cell lymphomas: Relation to NF-κB function in normal B cells. Biomedicines. 2022;10(10):2450.
21. Johnson PW, Balasubramanian S, Hodkinson B, Shreeve SM, Sun S, Srinivasan S, et al. Clinical impact of ibrutinib plus R-CHOP in untreated DLBCL coexpressing BCL2 and MYC in the phase 3 PHOENIX trial. Blood Advances. 2023;7(10):2008-17.
22. Younes A, Sehn LH, Johnson P, Zinzani PL, Hong X, Zhu J, et al. Randomized phase III trial of ibrutinib and rituximab plus cyclophosphamide, doxorubicin, vincristine, and prednisone in non–germinal center B-cell diffuse large B-cell lymphoma. Journal of Clinical Oncology. 2019;37(15):1285-95.
23. Studencka-Turski M, Maubach G, Feige MH, Naumann M. Constitutive activation of nuclear factor kappa B-inducing kinase counteracts apoptosis in cells with rearranged mixed lineage leukemia gene. Leukemia. 2018;32(11):2498-501.
24. Burley TA, Kennedy E, Broad G, Boyd M, Li D, Woo T, et al. Targeting the Non-Canonical NF-κB Pathway in Chronic Lymphocytic Leukemia and Multiple Myeloma. Cancers (Basel). 2022;14(6).
25. Haselager M, Thijssen R, West C, Young L, Van Kampen R, Willmore E, et al. Regulation of Bcl-XL by non-canonical NF-κB in the context of CD40-induced drug resistance in CLL. Cell Death & Differentiation. 2021;28(5):1658-68.
26. Froehlich TC, Müller-Decker K, Braun JD, Albrecht T, Schroeder A, Gülow K, et al. Combined inhibition of Bcl-2 and NFκB synergistically induces cell death in cutaneous T-cell lymphoma. Blood. 2019;134(5):445-55.
27. Bojarczuk K, Wienand K, Ryan JA, Chen L, Villalobos-Ortiz M, Mandato E, et al. Targeted inhibition of PI3Kα/δ is synergistic with BCL-2 blockade in genetically defined subtypes of DLBCL. Blood. 2019;133(1):70-80.
28. Elmore S. Apoptosis: a review of programmed cell death. Toxicol Pathol. 2007;35(4):495-516.
29. Cavalcante GC, Schaan AP, Cabral GF, Santana-da-Silva MN, Pinto P, Vidal AF, et al. A Cell's Fate: An Overview of the Molecular Biology and Genetics of Apoptosis. International Journal of Molecular Sciences. 2019;20(17):4133.
30. Monni O, Franssila K, Joensuu H, Knuutila S. BCL2 overexpression in diffuse large B-cell lymphoma. Leuk Lymphoma. 1999;34(1-2):45-52.
31. Morschhauser F, Feugier P, Flinn IW, Gasiorowski R, Greil R, Illés Á, et al. A phase 2 study of venetoclax plus R-CHOP as first-line treatment for patients with diffuse large B-cell lymphoma. Blood. 2021;137(5):600-9.
32. Davids MS, Roberts AW, Seymour JF, Pagel JM, Kahl BS, Wierda WG, et al. Phase I First-in-Human Study of Venetoclax in Patients With Relapsed or Refractory Non-Hodgkin Lymphoma. J Clin Oncol. 2017;35(8):826-33.

436 33. Bose P, Gandhi V, Konopleva M. Pathways and mechanisms of venetoclax resistance.
437 Leukemia & lymphoma. 2017;58(9):2026-39.
438 34. Victoria MS, Anna D, Kristina H, Daniela B, Ross J, Lisa K, et al. Specific interactions of
439 BCL-2 family proteins mediate sensitivity to BH3-mimetics in diffuse large B-cell lymphoma.
440 Haematologica. 2020;105(8):2150-63.
441 35. Certo M, Moore VDG, Nishino M, Wei G, Korsmeyer S, Armstrong SA, et al. Mitochondria
442 primed by death signals determine cellular addiction to antiapoptotic BCL-2 family members.
443 Cancer Cell. 2006;9(5):351-65.
444 36. Deng J, Carlson N, Takeyama K, Dal Cin P, Shipp M, Letai A. BH3 profiling identifies three
445 distinct classes of apoptotic blocks to predict response to ABT-737 and conventional
446 chemotherapeutic agents. Cancer cell. 2007;12(2):171-85.
447 37. Olesinski EA, Bhatia KS, Mahesh AN, Rosli S, Mohamed JS, Jen WY, et al. BH3 profiling
448 identifies BCL-2 dependence in adult patients with early T-cell progenitor acute lymphoblastic
449 leukemia. Blood Advances. 2023;7(12):2917-23.
450 38. Butterworth M, Pettitt A, Varadarajan S, Cohen GM. BH3 profiling and a toolkit of BH3-
451 mimetic drugs predict anti-apoptotic dependence of cancer cells. British Journal of Cancer.
452 2016;114(6):638-41.
453 39. Cloete I, Smith VM, Jackson RA, Pepper A, Pepper C, Vogler M, et al. Computational
454 modeling of DLBCL predicts response to BH3-mimetics. NPJ Systems Biology and Applications.
455 2023;9(1):23.
456 40. Mitchell S, Tsui R, Tan ZC, Pack A, Hoffmann A. The NF-κB multidimer system model: A
457 knowledge base to explore diverse biological contexts. Science signaling.
458 2023;16(776):eabo2838.
459 41. Norris R, Jones J, Mancini E, Chevassut T, Simoes FA, Pepper C, et al. Patient-specific
460 computational models predict prognosis in B cell lymphoma by quantifying pro-proliferative and
461 anti-apoptotic signatures from genetic sequencing data. Blood Cancer Journal. 2024;14(1):105.
462 42. Almaden JV, Tsui R, Liu YC, Birnbaum H, Shokhirev MN, Ngo KA, et al. A pathway switch
463 directs BAFF signaling to distinct NFκB transcription factors in maturing and proliferating B cells.
464 Cell Rep. 2014;9(6):2098-111.
465 43. Bian Y, Li L, Dong M, Liu X, Kaneko T, Cheng K, et al. Ultra-deep tyrosine
466 phosphoproteomics enabled by a phosphotyrosine superbinder. Nat Chem Biol. 2016;12(11):959-
467 66.
468 44. Mitchell S, Roy K, Zangle TA, Hoffmann A. Nongenetic origins of cell-to-cell variability in
469 B lymphocyte proliferation. Proceedings of the National Academy of Sciences.
470 2018;115(12):E2888-E97.
471 45. Rackauckas C, Nie Q. Differentialequations. jl–a performant and feature-rich ecosystem
472 for solving differential equations in julia. Journal of open research software. 2017;5(1):15-.
473 46. Deng W, Clipson A, Liu H, Huang Y, Dobson R, Wang M, et al. Variable Responses of
474 MYC Translocation Positive Lymphoma Cell Lines To Different Combinations of Novel Agents:
475 Impact of BCL2 Family Protein Expression. Translational Oncology. 2018;11(5):1147-54.
476 47. Quentmeier H, Amini RM, Berglund M, Dirks WG, Ehrentraut S, Geffers R, et al. U-2932:
477 two clones in one cell line, a tool for the study of clonal evolution. Leukemia. 2013;27(5):1155-64.
478 48. Tromp JM, Tonino SH, Elias JA, Jaspers A, Luijks DM, Kater AP, et al. Dichotomy in NF-
479 κB signaling and chemoresistance in immunoglobulin variable heavy-chain-mutated versus
480 unmutated CLL cells upon CD40/TLR9 triggering. Oncogene. 2010;29(36):5071-82.
481 49. Estupiñán HY, Bouderlique T, He C, Berglöf A, Cappelleri A, Frengen N, et al. In BTK,
482 phosphorylated Y223 in the SH3 domain mirrors catalytic activity, but does not influence biological
483 function. Blood Adv. 2024;8(8):1981-90.

50. Homig-Holzel C, Hojer C, Rastelli J, Casola S, Strobl LJ, Müller W, et al. Constitutive CD40 signaling in B cells selectively activates the noncanonical NF-κB pathway and promotes lymphomagenesis. The Journal of experimental medicine. 2008;205(6):1317-29.
51. Zhao B, Barrera LA, Ersing I, Willox B, Schmidt SC, Greenfeld H, et al. The NF-κB genomic landscape in lymphoblastoid B cells. Cell reports. 2014;8(5):1595-606.
52. Zou Z, Ohta T, Oki S. ChIP-Atlas 3.0: a data-mining suite to explore chromosome architecture together with large-scale regulome data. Nucleic Acids Research. 2024:gkae358.
53. Coiffier B, Sarkozy C. Diffuse large B-cell lymphoma: R-CHOP failure-what to do? Hematology Am Soc Hematol Educ Program. 2016;2016(1):366-78.
54. Raut LS, Chakrabarti PP. Management of relapsed-refractory diffuse large B cell lymphoma. South Asian J Cancer. 2014;3(1):66-70.
55. Prescott JA, Cook SJ. Targeting IKKβ in Cancer: Challenges and Opportunities for the Therapeutic Utilisation of IKKβ Inhibitors. Cells. 2018;7(9):115.
56. Eluard B, Nuan-Aliman S, Faumont N, Collares D, Bordereaux D, Montagne A, et al. The alternative RelB NF-κB subunit is a novel critical player in diffuse large B-cell lymphoma. Blood. 2022;139(3):384-98.
57. Kapoor I, Bodo J, Hill BT, Hsi ED, Almasan A. Targeting BCL-2 in B-cell malignancies and overcoming therapeutic resistance. Cell Death & Disease. 2020;11(11):941.
58. Waclawiczek A, Leppä A-M, Renders S, Stumpf K, Reyneri C, Betz B, et al. Combinatorial BCL2 Family Expression in Acute Myeloid Leukemia Stem Cells Predicts Clinical Response to Azacitidine/Venetoclax. Cancer Discovery. 2023;13(6):1408-27.
59. Woyach JA, Johnson AJ. Targeted therapies in CLL: mechanisms of resistance and strategies for management. Blood, The Journal of the American Society of Hematology. 2015;126(4):471-7.
60. Liu H, Yang J, Yuan Y, Xia Z, Chen M, Xie L, et al. Regulation of Mcl-1 by constitutive activation of NF-kappaB contributes to cell viability in human esophageal squamous cell carcinoma cells. BMC Cancer. 2014;14(1):98.
61. Faumont N, Taoui O, Collares D, Jais J-P, Leroy K, Prévaud L, et al. C-rel is the pivotal NF-κB subunit in germinal center diffuse Large b-cell lymphoma: a LYSA study. Frontiers in Oncology. 2021;11:638897.
62. Liu T, Xu F, Thieme E, Lam V, Fan G, Nikolaenko L, et al. Pharmacologic targeting MCL1 with AZD5991 induces apoptosis and mitochondrial dysfunction in non-Hodgkin lymphoma (NHL) cells. Blood. 2020;136:33.
63. Desai P, Lonial S, Cashen A, Kamdar M, Flinn I, O'Brien S, et al. A Phase 1 First-in-Human Study of the MCL-1 Inhibitor AZD5991 in Patients with Relapsed/Refractory Hematologic Malignancies. Clinical Cancer Research. 2024:OF1-OF12.
64. Moore VDG, Letai A. BH3 profiling–measuring integrated function of the mitochondrial apoptotic pathway to predict cell fate decisions. Cancer letters. 2013;332(2):202-5.

523 **Figure Legends**

524 **Figure 1.** Summary of existing knowledge of links between the Tumour Microenvironment (TME),
525 NF-κB dimers, and BCL2-family proteins in lymphoma. The canonical NF-κB pathway (green) is
526 mediated in part by B-cell receptor (BCR) signaling. BCR signaling transduces signals through
527 Bruton's tyrosine kinase (BTK), and NF-κB essential modulator (NEMO), to primarily activate RelA-
528 and cRel-containing NF-κB dimers. Single cell RNA sequencing has revealed that the primary
529 impact of the TME on DLBCL cells is through the non-canonical NF-κB pathway (purple).
530 Macrophages (Mϕ), dendritic cells (DC), and cancer associated fibroblasts (CAFS), activate non-
531 canonical signaling through B cell-activating factor receptor (BAFFR). T cells in the TME secrete
532 CD40 ligand. Both BAFFR and CD40 activation lead to stabilization of NF-κB-inducing kinase (NIK)
533 and activation of RelB-containing NF-κB dimers. While RelB activity has been shown to upregulate
534 BCLXL in chronic lymphocytic leukemia, and there are frequently reported links between NF-κB and
535 BCL2, it is unknown which NF-κB dimers induce which BCL2-family proteins (indicated by gray
536 arrows), and how this drives response to therapies in the context of the DLBCL TME.

537 **Figure 2.** NF-κB and BCL2 'fingerprinting' predicts sensitivities to inhibition of non-canonical NF-κB
538 and BCL2 in Diffuse Large B cell Lymphoma (DLBCL). (A) Representative dot plots of RelA and RelB
539 Median Fluorescence Intensity (MFI) values for the DLBCL cell lines SUDHL8, SUDHL10, U2932, and
540 RIVA. Workflow pipeline for the productions of NF-κB fingerprints. (B) Relative RelA and RelB
541 expression levels measured with flow cytometry, in the cell lines RIVA, U2932, SUDHL8 and
542 SUDHL10 as fingerprints, with dots representing the median in a single experiment, also shown as
543 probability density curves (right and top). (C) Bar graphs of RelA and RelB median fluorescence
544 intensity (MFI) values as mean ± standard deviation of two independent experiments. (*$P$< 0.05; one-
545 way ANOVA with Tukey's comparisons test). (D) Cell viability in response to 0.125-100μM of Amgen16
546 in the indicated DLBCL cell lines post a 24-hour treatment, error bars representing the mean ±
547 standard deviation of three independent experiments, normalized to the untreated control. (E) $LC_{50}$
548 values for the indicated cell lines in response to Amgen16 with mean indicated, three independent
549 experiments *(**P<0.01, ***P<0.001 unpaired T-test)*. (F) Relative MCL1, and BCL2, and BCLXL
550 expression levels measured with flow cytometry, in the cell lines RIVA, U2932, SUDHL8 and
551 SUDHL10 as fingerprints, with dots representing the median in a single experiment, also shown as
552 probability density curves (right and top). (G) Bar graphs of MCL1, and BCL2, and BCLXL median
553 fluorescence intensity (MFI) values as mean ± standard deviation of three independent experiments.
554 *(*P<0.05, **P< 0.01, ***P<0.001, ****P<0.0001; one-way ANOVA with Tukey's comparisons test*). (H)
555 Cell viability in response to 0.0001-100μM of ABT199 (venetoclax) in the indicated DLBCL cell lines,
556 post a 24-hour treatment, error bars representing the mean ± standard deviation of three
557 independent experiments, normalized to the untreated control. (I) $LC_{50}$ values for the indicated cell
558 lines in response to ABT199 with mean indicated, of three independent experiments *(**P<0.01,*
559 ****P<0.001 unpaired T-test)*.

560 **Figure 3.** Differential BCL2 family abundance in the sub-clonal cell line U2932 predicts differential
561 responses to ABT199 (venetoclax), TME mimicking hCD40L-3T3 co-culture confers resistance to
562 BCL2 inhibition. (A) Flow cytometry dot plot showing the distinct levels of CD20 Median
563 Fluorescence Intensity (MFI) in the U2932 subclones R1 and R2. (B) Cell viability in response to
564 0.0001-100μM of ABT199in the indicated U2932 subclones R1 and R2, post 24-hour treatment, error
565 bars representing the mean ± standard deviation of three independent experiments, normalized to
566 the untreated control. (C) Bar graphs of MCL1, and BCL2, and BCLXL median fluorescence intensity
567 (MFI) values as mean ± standard deviation of three independent experiments (****$P$<0.0001;
568 unpaired t-test). (C) Cell viability in response to 0.0001-100μM of ABT199in the indicated U2932
569 subclones R1 and R2, post 24-hour treatment, error bars representing the mean ± standard deviation
570 of three independent experiments, normalized to the untreated control. (D) Schematic of the co-
571 culture system used. U2932 cells were co-cultured with hCD40L-3T3 cells prior to treatment with
572 increasing doses of ABT199. (E) Viability of U2932 cells cultured for 24 hours with or without CD40-
573 Ligand NIH3T3 in the presence of 0.0001-100μM of ABT199. Error bars representing the mean ±
574 standard deviation of three independent experiments, normalized to the untreated control *(**P<0.01,*
575 *****P<0.001 multiple unpaired T-tests using the Holm-Šídák corrections test)*. (F) LC50 values for the
576 U2932 cell line in monoculture vs co-culture with hCD40L-3T3 in response to ABT199, with error bars
577 representing the mean ± standard deviation of three independent experiments*(**P<0.01, unpaired T-*
578 *test). (G)* MCL1, BCL2, and BCLXL levels, shown as fold changes of 24-hour stimulation with hCD40L-
579 3T3 cells to unstimulated control in U2932 cells with error bars representing the mean ± standard
580 deviation of five independent experiments *(*P<0.05, **P<0.01 one-way ANOVA with Tukey's*
581 *comparisons test)*.
582

583 **Figure 4.** Tumor microenvironment-mimicking co-culture induced resistance to BH3-mimetics in
584 Diffuse Large B Cell Lymphoma (DLBCL) cell lines. (A) Viability of RIVA cells cultured for 24 hours with
585 or without hCD40L-3T3 cells in the presence of 0.0001-100μM of the BCL-2 inhibitor ABT199
586 (venetoclax). Error bars representing the mean ± standard deviation of three independent
587 experiments, normalized to the untreated control. (B) $LC_{50}$ values for RIVA in each condition with error
588 bars representing the mean ± standard deviation of three independent experiments, normalized to
589 the untreated control (*$P<0.05$, unpaired T-test). (C) MCL1, BCL2, and BCLXL levels, shown as fold
590 changes of 24-hour stimulation with hCD40L-3T3 cells to unstimulated control in RIVA with error bars
591 representing the mean ± standard deviation of five independent experiments *(**$P<0.01$, ***$P<0.001$*
592 one-way ANOVA with Tukey's comparisons test. (D) Viability of SUDHL8 cells cultured for 24 hours
593 with or without hCD40L-3T3 cells in the presence of 0.0001-100μM of the BCLXL inhibitor A1331852.
594 Error bars representing the mean ± standard deviation of three independent experiments, normalized
595 to the untreated control. (E) $LC_{50}$ values for SUDHL8 in each condition with error bars representing
596 the mean ± standard deviation of three independent experiments, normalized to the untreated
597 control (***$P<0.001$, unpaired T-test). (F) MCL1, BCL2, and BCLXL levels, shown as fold changes of
598 24-hour stimulation with hCD40L-3T3 cells to unstimulated control in SUDHL8 with error bars
599 representing the mean ± standard deviation of five independent experiments *(*$P<0.05$,* one-way
600 ANOVA with Tukey's comparisons test).

601 **Figure 5.** Immunofluorescence microscopy reveals differential NF-κB basal RelA activity in Diffuse
602 Large B-cell Lymphoma (DLBCL) cell lines. (A) Schematic of the canonical and non-canonical NF-κB
603 signaling pathway illustrating how non-canonical NF-κB activation results in the induction of BCLXL
604 and how elevated basal canonical signaling induces multiple negative regulators of NF-κB which may
605 contribute to cell line specific induction of MCL1. (B) Representative immunofluorescence
606 microscopy following staining in RIVA cells for RelA (NF-κB), DAPI (nucleus), actin (cytoplasm), to
607 measure nuclear and cytoplasmic subcellular localization. (C) Quantification immunofluorescence
608 microscopy showing nuclear to cytoplasmic ratio of cRel and RelA in single cells. Data shows a
609 representative replicate in the indicated cell lines. Violin width indicates data density. (D)
610 Quantification of the nuclear to cytoplasmic ratio of cRel (top) and RelA (bottom) as bar graphs with
611 error bars of the mean ± standard deviation of three independent experiments in RIVA, U2932 and
612 SUDHL8 (*P<0.05; One-Way ANOVA).
613

614 **Figure 6.** Co-culture with hCD40L-3T3 cells upregulates NF-κB RelB and BCLXL in DLBCL, and
615 selectively upregulates NF-κB cRel and MCL1 through signaling crosstalk when NF-κB RelA is
616 chronically active. (A) Abundances of the heterodimers RelA:p50 (left) and cRel:p50 (right) bound to
617 inhibiting NF-κB proteins (IκB), as simulated by computational modeling for basal canonical NF-κB
618 activation state in RIVA, and high basal activation state in SUDHL8. (B) Computational modeling
619 results showing the nuclear abundance of the indicated NF-κB dimers in a simulation with low basal
620 nuclear RelA (RIVA, pink), and a simulation high basal nuclear RelA (SUDHL8, teal). The mean (line)
621 and standard deviation (shaded region) of 25 cells is indicated. (C) Schematic demonstrating the
622 mechanism by which NF-κB contributes to the induction of BCLXL in a cell line with normal basal
623 signaling (RIVA) upon stimulation with CD40L (right). hCD40L-3T3 mediated activation of NIK results
624 in p100 processing into p52, leading to nuclear translocation of RelB:p52 and increased expression
625 of BCLXL. Gray = inactive pathways and low abundance proteins, color = active pathways and
626 predominant complexes. (D) Schematic demonstrating how crosstalk emerges between CD40, NIK,
627 cRel, and MCL1. Increase basal RelA results in increase p100, and IκBδ (left). hCD40L-3T3 mediated
628 activation of NIK results in processing of IκBδ and release of cRel:p50, which translocates to the
629 nucleus and potentially upregulates expression of MCL1 (right). Gray = inactive pathways and low
630 abundance proteins, color = active pathways and predominant complexes. (E-F) Quantification of
631 immunofluorescence microscopy in RIVA (E) and SUDHL8 (F) cells showing nuclear to cytoplasmic
632 ratio of RelA, RelB and cRel. Data post 24 hours of monoculture and hCD40L-3T3co-culture is shown
633 side by side. Single cells of a representative replicate are shown (left), with violin width indicating
634 data density. Quantification of the nuclear to cytoplasmic ratio of RelA, RelB and cRel is shown as
635 bar graphs (right) with error bars displaying the mean ± standard deviation of three independent
636 experiments (*$P<0.05$, **$P<0.01$; unpaired t-test). (G) Schematic of the co-culture system used,
637 following 24 hours of treatment with 0.0001-100μM of the BCLXL inhibitor A1331852 ± 0.1μM of the

638 Bruton's Kinase (BTK) inhibitor Ibrutinib. (H) Cell viability of SUDHL8 in response to 0.0001-100μM of
639 the BCLXL inhibitor A1331852 post a 24-hour treatment in monoculture, post a 24-hour hCD40L-
640 3T3co-culture or post a 24-hour hCD40L-3T3 co-culture with the addition of 0.1μM of the BTK
641 inhibitor, Ibrutinib. $LC_{50}$ values for each condition is shown (right) with error bars representing the
642 mean ± standard deviation of three independent experiments, normalized to the untreated control
643 (****P<0.001* one-way ANOVA with Tukey's comparisons test).
644

645 **Figure 7.** IκBε knock-out mouse model reveals cRel-dependent induction of MCL1. (A) NF-κB ChIP-
646 seq data from Zhao et al. 2014 (52) showing binding of the indicated NF-κB subunits around the
647 transcription start site (TSS) of the indicated anti-apoptotic genes in lymphoblastoid B cell line. A 1kb
648 window around the TSS is indicated. (B) Model-based Analysis for ChIP-Seq 2 (MACS2) scores for the
649 indicated NF-κB subunits within 1kb of the MCL1 promoter across all ChIP-Seq datasets reported in
650 ChIP Atlas Zou et al. 2024 (52), after outlier removal using ROUT method (q=1%, ****$P<0.0001$). (C)
651 Schematic of normal basal NF-κB signaling (left), schematic of NF-κB signaling predicting the
652 unknown effect of IκBε$^{-/-}$ on cRel and MCL-1 induction. (D) Computational modelling simulation of
653 RelA and cRel abundance in IκBε$^{-/-}$ and IκBα$^{κB/κB}$ demonstrated as fold changes normalized to wild-
654 type. Error bars represent the mean and ± standard deviation of 25 cells (***$P<0.001$, unpaired t-test).
655 (E) RelA and cRel abundances in IκBε$^{-/-}$ and IκBα$^{κB/κB}$ cells derived from primary splenocytes,
656 demonstrated as fold changes to wild-type, error bars representing the mean ± standard deviation.
657 (F) Experimental pipeline showing the workflow of isolating and purifying primary B cells from wild
658 type, IκBε$^{-/-}$ and IκBα$^{κB/κB}$ mouse genotypes. (G) Abundances of MCL1 and BCLXL acquired with flow
659 cytometry in primary B cells isolated and purified from IκBε$^{-/-}$ (left) and IκBα$^{κB/κB}$ (right) mouse
660 genotypes, demonstrated as fold changes normalized to wild-type. Error bars represent the mean ±
661 standard deviation of three independent experiments (*$P<0.05$, unpaired t-test).
662

**Figure 8.** Targeting the NF-κB inducing kinase (NIK) to overcome tumor microenvironment (TME) resistance in Diffuse large B cell lymphoma (DLBCL). (A) Overview of signaling between TME, NF-κB, and BCL2-family proteins indicating interactions revealed here with dashed lines, and NIK-inhibitor Amgen16 displayed in red. (B) Schematic of the co-culture system used, following 24 hours of treatment with 0.0001-100μM of venetoclax (ABT199) or A1331852 ± 50μM of the NIK inhibitor Amgen16 . (C) Cell viability of SUDHL8 in response to 0.0001-100μM of A1331852 post a 24-hour treatment in monoculture, post 24-hour co-culture on hCD40L-3T3 cells or post 24-hour hCD40L-3T3 co-culture with the addition of 50μM of the NIK inhibitor Amgen16. $LC_{50}$ values for each condition is shown (right) with error bars representing the mean ± standard deviation of three independent experiments, normalized to the untreated control (****P<0.001* one-way ANOVA with Tukey's comparisons test). (D) U2932 and (E) RIVA cells in response to 0.0001-100μM of ABT199 in the cell lines post a 24-hour treatment in monoculture, post a 24-hour hCD40L-3T3 co-culture or post 24-hour hCD40L-3T3 co-culture with the addition of 50μM of the NIK inhibitor, Amgen16. $LC_{50}$ values for each condition is shown (right) with error bars representing the mean ± standard deviation of three independent experiments, normalized to the untreated control (**P<0.05, **P<0.01* one-way ANOVA with Tukey's comparisons test.

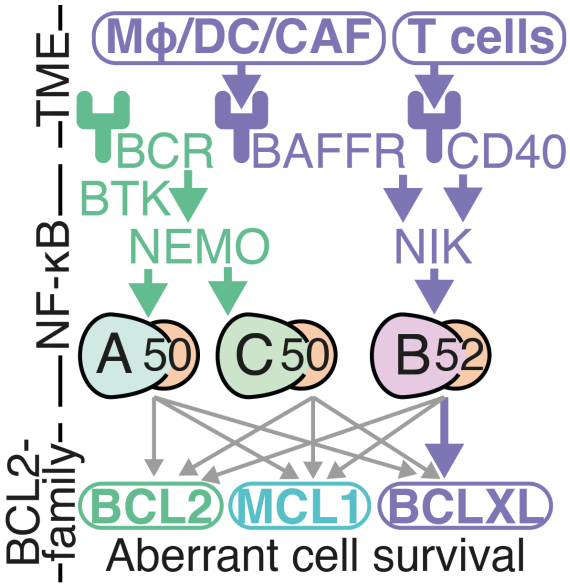
TME
Mϕ/DC/CAF
T cells
BCR
BAFFR
CD40
NF-κB
BTK
NEMO
NIK
A 50
C 50
B 52
BCL2-family
BCL2
MCL1
BCLXL
Aberrant cell survival

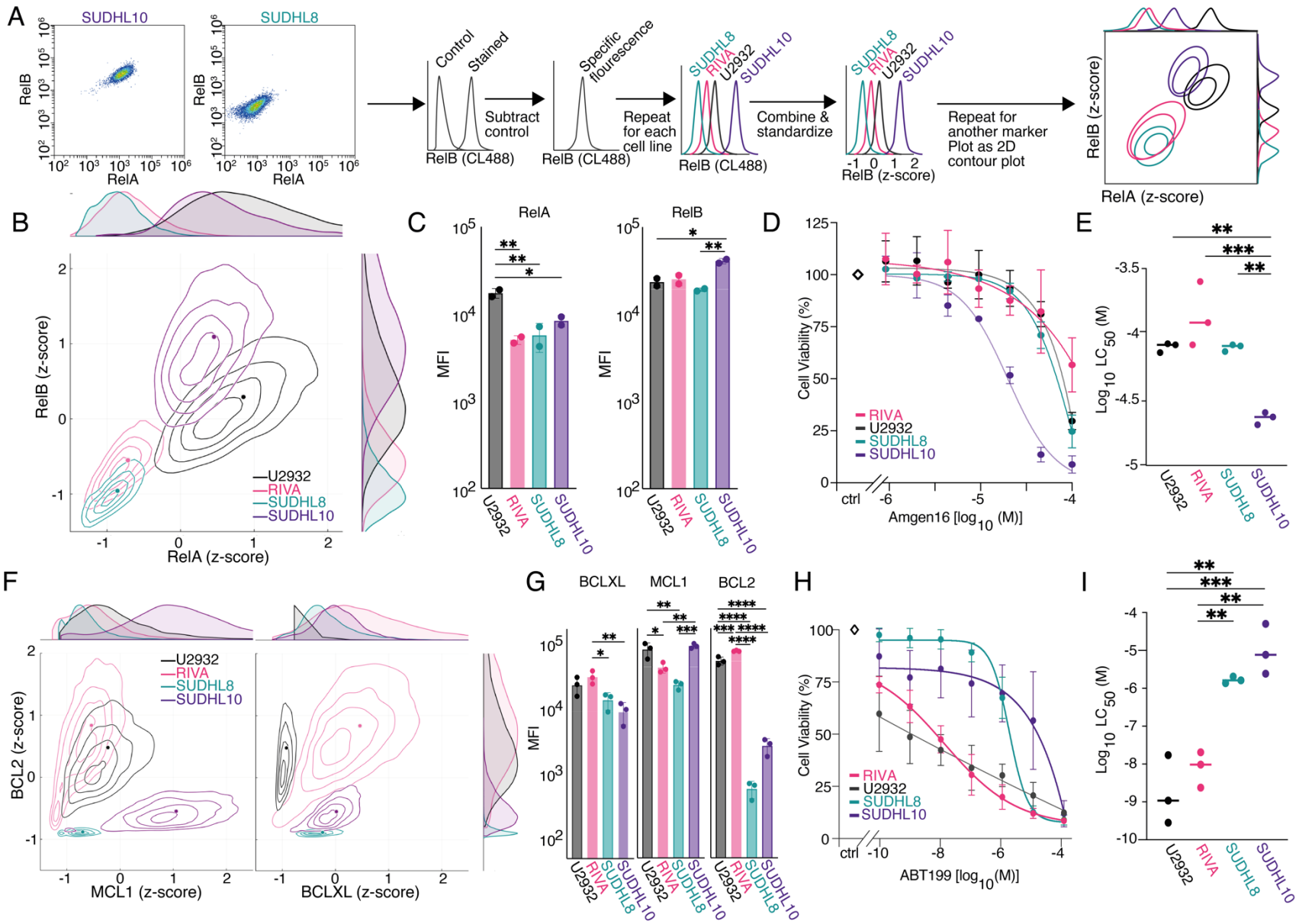
A
SUDHL10
SUDHL8
RelB
RelA
Control
Stained
Subtract control
RelB (CL488)
Specific flourescence
Repeat for each cell line
SUDHL8
RIVA
U2932
SUDHL10
Combine & standardize
RelB (z-score)
Repeat for another marker Plot as 2D contour plot
RelA (z-score)
B
U2932
RIVA
SUDHL8
SUDHL10
C
RelA
RelB
MFI
D
Cell Viability (%)
Amgen16 [log10 (M)]
ctrl
E
Log10 LC50 (M)
F
BCL2 (z-score)
MCL1 (z-score)
BCLXL (z-score)
G
BCLXL
MCL1
BCL2
H
ABT199 [log10(M)]
I

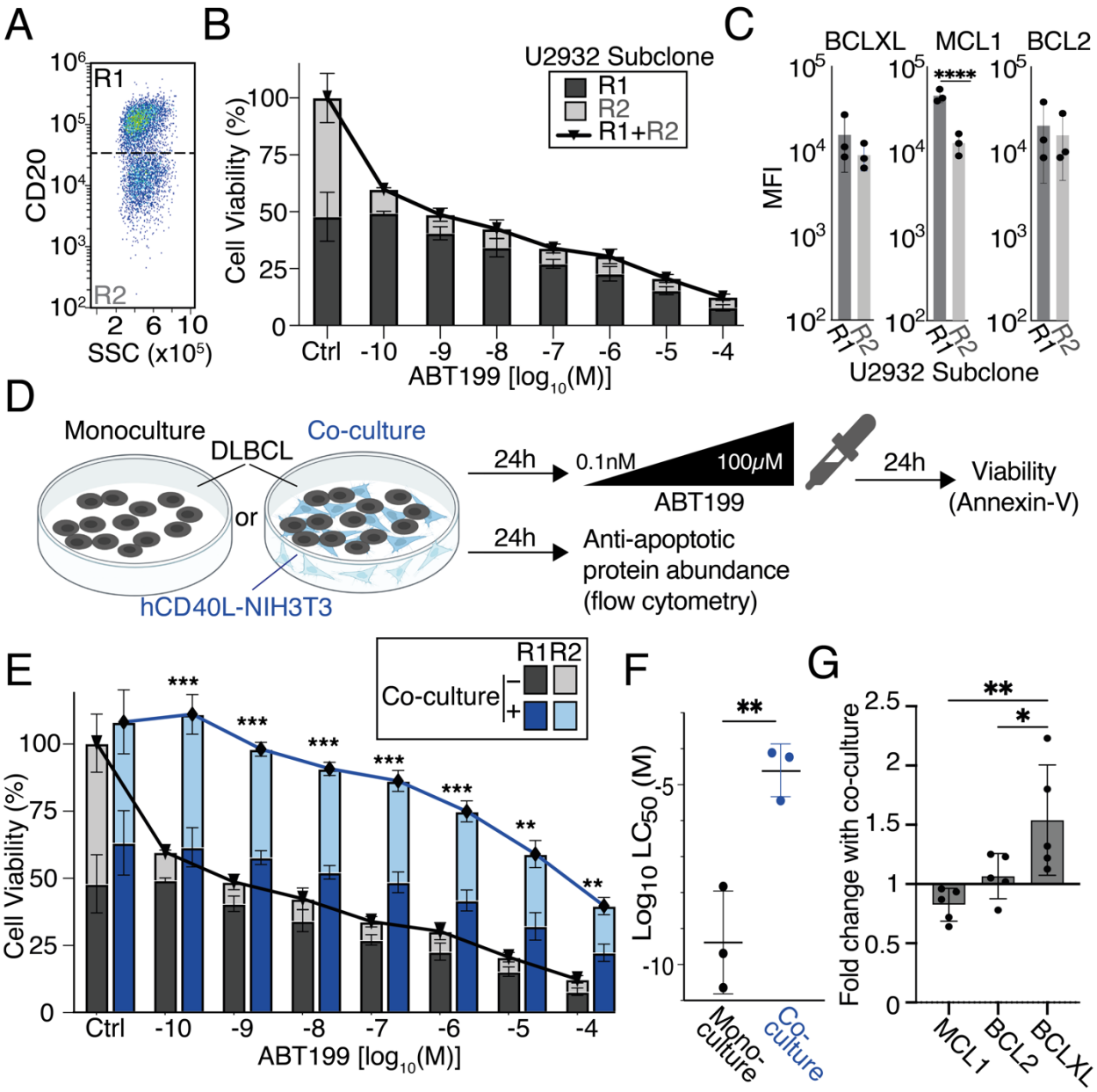
A
R1
R2
CD20
SSC (x10^5)
B
U2932 Subclone
R1
R2
R1+R2
Cell Viability (%)
Ctrl
-10
-9
-8
-7
-6
-5
-4
ABT199 [log10(M)]
C
BCLXL
MCL1
BCL2
MFI
****
R1
R2
U2932 Subclone
D
Monoculture
DLBCL
Co-culture
or
hCD40L-NIH3T3
24h
0.1nM
100μM
ABT199
24h
Viability
(Annexin-V)
24h
Anti-apoptotic
protein abundance
(flow cytometry)
E
R1R2
Co-culture
–
+
Cell Viability (%)
Ctrl
-10
-9
-8
-7
-6
-5
-4
ABT199 [log10(M)]
F
Log10 LC50 (M)
Mono-
culture
Co-
culture
G
Fold change with co-culture
MCL1
BCL2
BCLXL

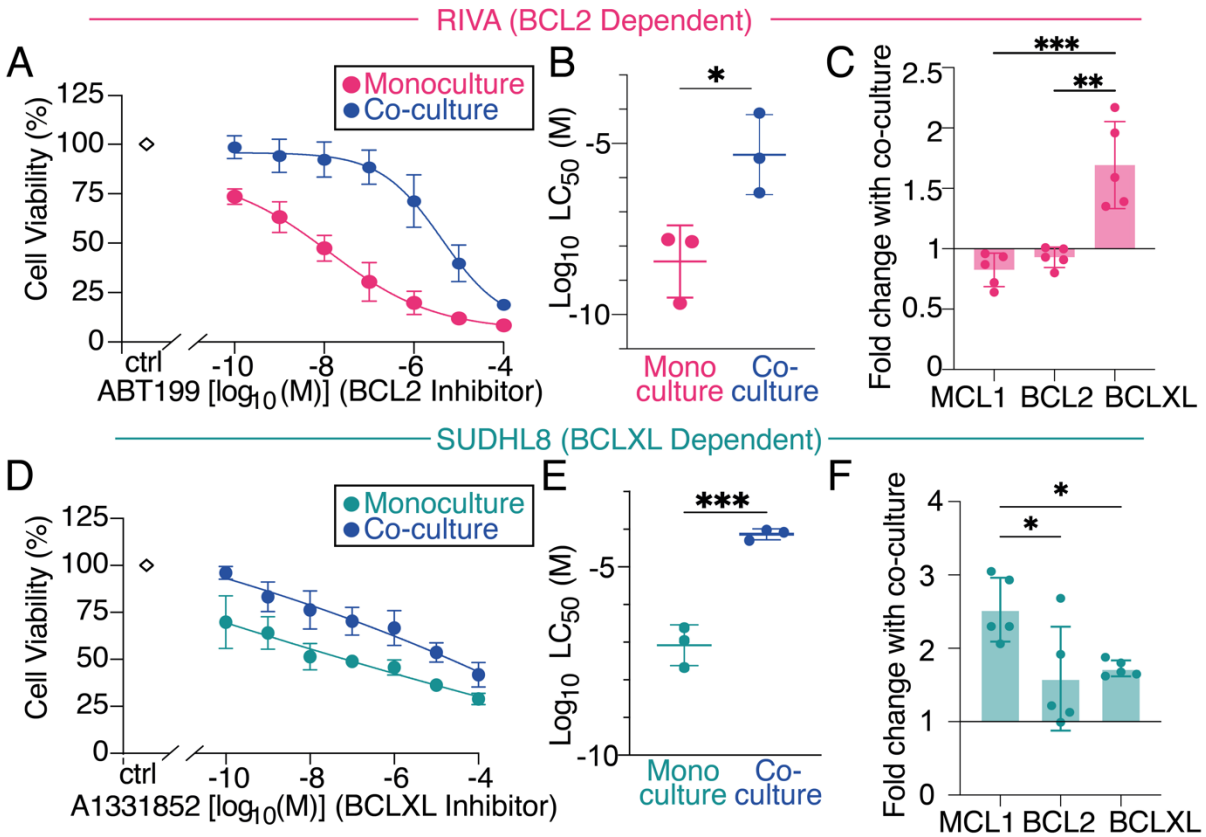
RIVA (BCL2 Dependent)
A
Monoculture
Co-culture
Cell Viability (%)
125
100
75
50
25
0
ctrl
-10
-8
-6
-4
ABT199 [log10(M)] (BCL2 Inhibitor)
B
*
Log10 LC50 (M)
-5
-10
Mono culture
Co-culture
C
***
**
Fold change with co-culture
2.5
2
1.5
1
0.5
0
MCL1
BCL2
BCLXL
SUDHL8 (BCLXL Dependent)
D
Monoculture
Co-culture
Cell Viability (%)
125
100
75
50
25
0
ctrl
-10
-8
-6
-4
A1331852 [log10(M)] (BCLXL Inhibitor)
E
***
Log10 LC50 (M)
-5
-10
Mono culture
Co-culture
F
*
*
Fold change with co-culture
4
3
2
1
0
MCL1
BCL2
BCLXL

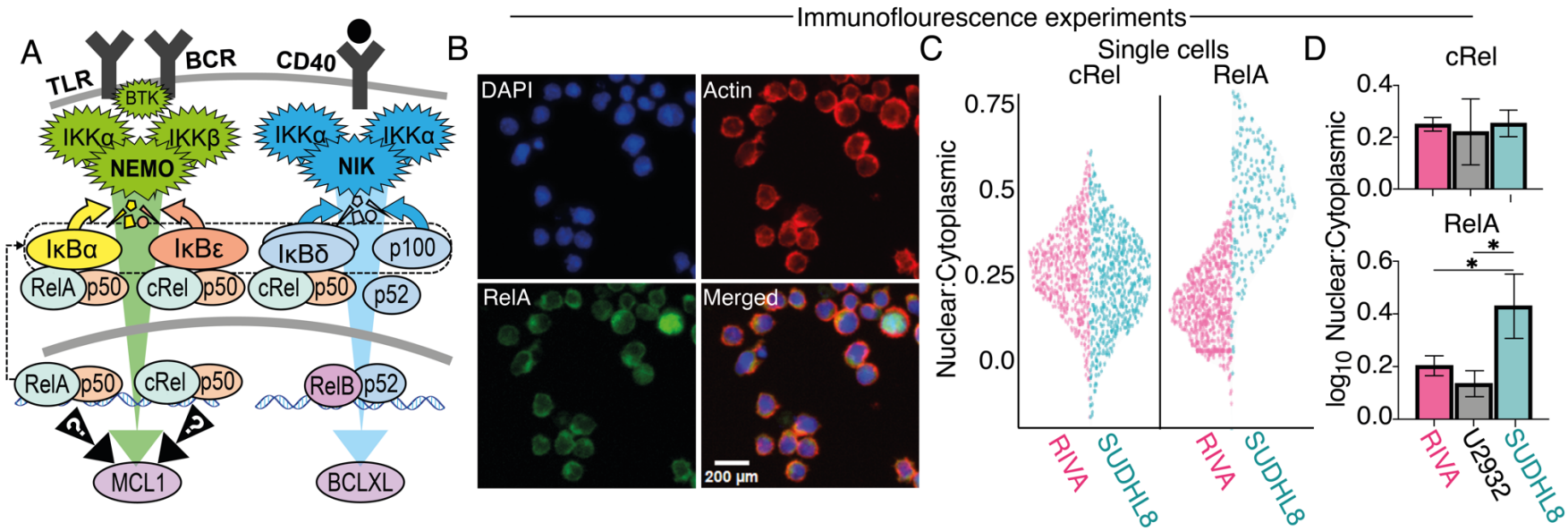
A
TLR
BCR
CD40
BTK
IKKα
IKKβ
NEMO
IKKα
IKKα
NIK
IκBα
IκBε
IκBδ
p100
RelA
p50
cRel
p50
cRel
p50
p52
RelA
p50
cRel
p50
RelB
p52
MCL1
BCLXL
Immunoflourescence experiments
B
DAPI
Actin
RelA
Merged
200 µm
C
Single cells
cRel
RelA
Nuclear:Cytoplasmic
0.75
0.5
0.25
0.0
RIVA
SUDHL8
RIVA
SUDHL8
D
cRel
RelA
log10 Nuclear:Cytoplasmic
0.4
0.2
0.0
0.6
0.4
0.2
0.0
*
*
RIVA
U2932
SUDHL8

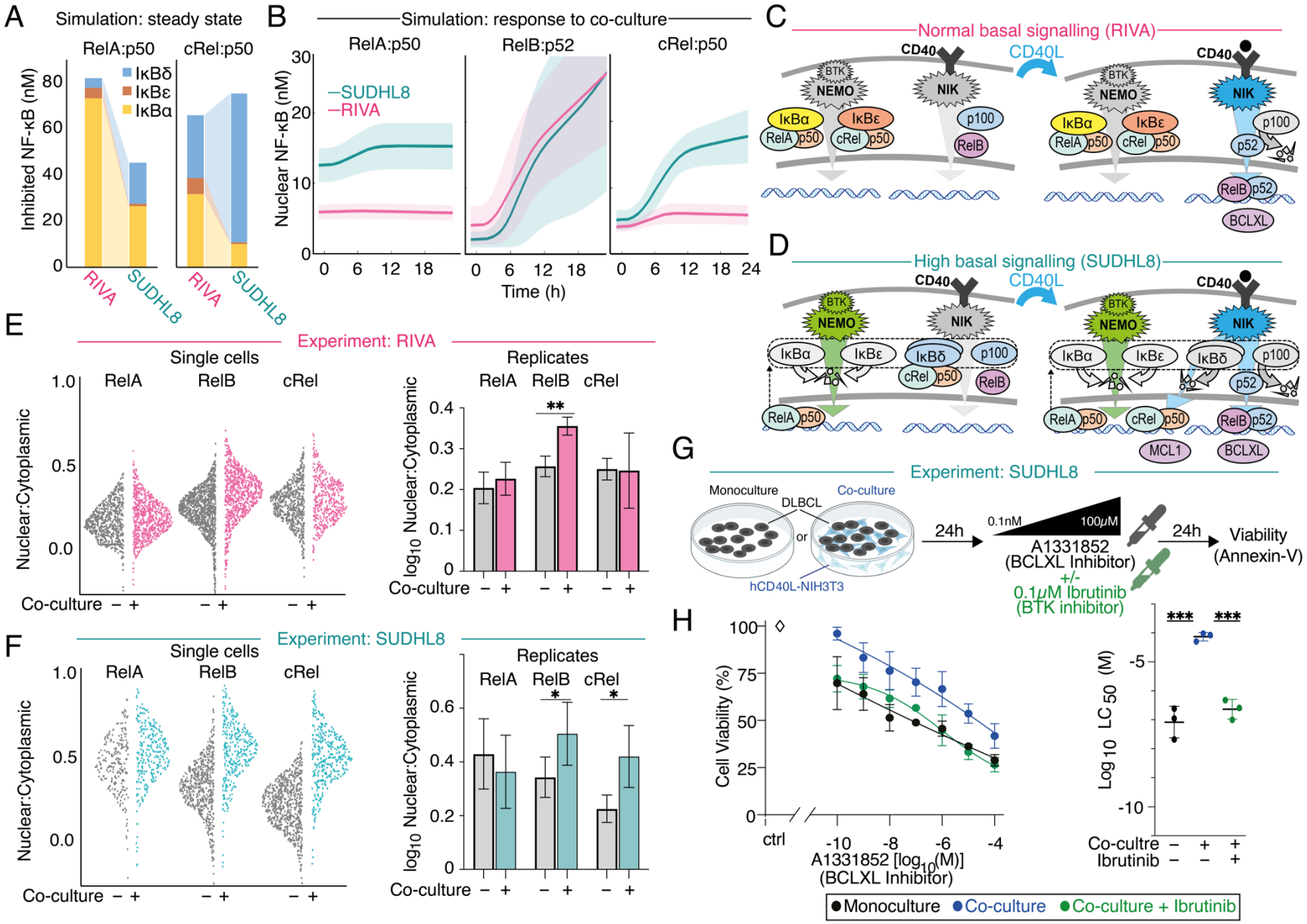
A
Simulation: steady state
RelA:p50
cRel:p50
IκBδ
IκBε
IκBα
Inhibited NF-κB (nM)
RIVA
SUDHL8
B
Simulation: response to co-culture
RelA:p50
RelB:p52
cRel:p50
SUDHL8
RIVA
Nuclear NF-κB (nM)
Time (h)
C
Normal basal signalling (RIVA)
CD40
CD40L
BTK
NEMO
NIK
IκBα
IκBε
RelA
p50
cRel
p100
RelB
p52
BCLXL
D
High basal signalling (SUDHL8)
IκBδ
MCL1
E
Experiment: RIVA
Single cells
Replicates
RelA
RelB
cRel
Nuclear:Cytoplasmic
log10 Nuclear:Cytoplasmic
Co-culture
F
Experiment: SUDHL8
G
Experiment: SUDHL8
Monoculture
Co-culture
DLBCL
or
hCD40L-NIH3T3
24h
0.1nM
100μM
A1331852
(BCLXL Inhibitor)
+/-
0.1μM Ibrutinib
(BTK inhibitor)
Viability
(Annexin-V)
H
Cell Viability (%)
ctrl
A1331852 [log10(M)]
(BCLXL Inhibitor)
Log10 LC50 (M)
Co-cultre
Ibrutinib
Monoculture
Co-culture
Co-culture + Ibrutinib

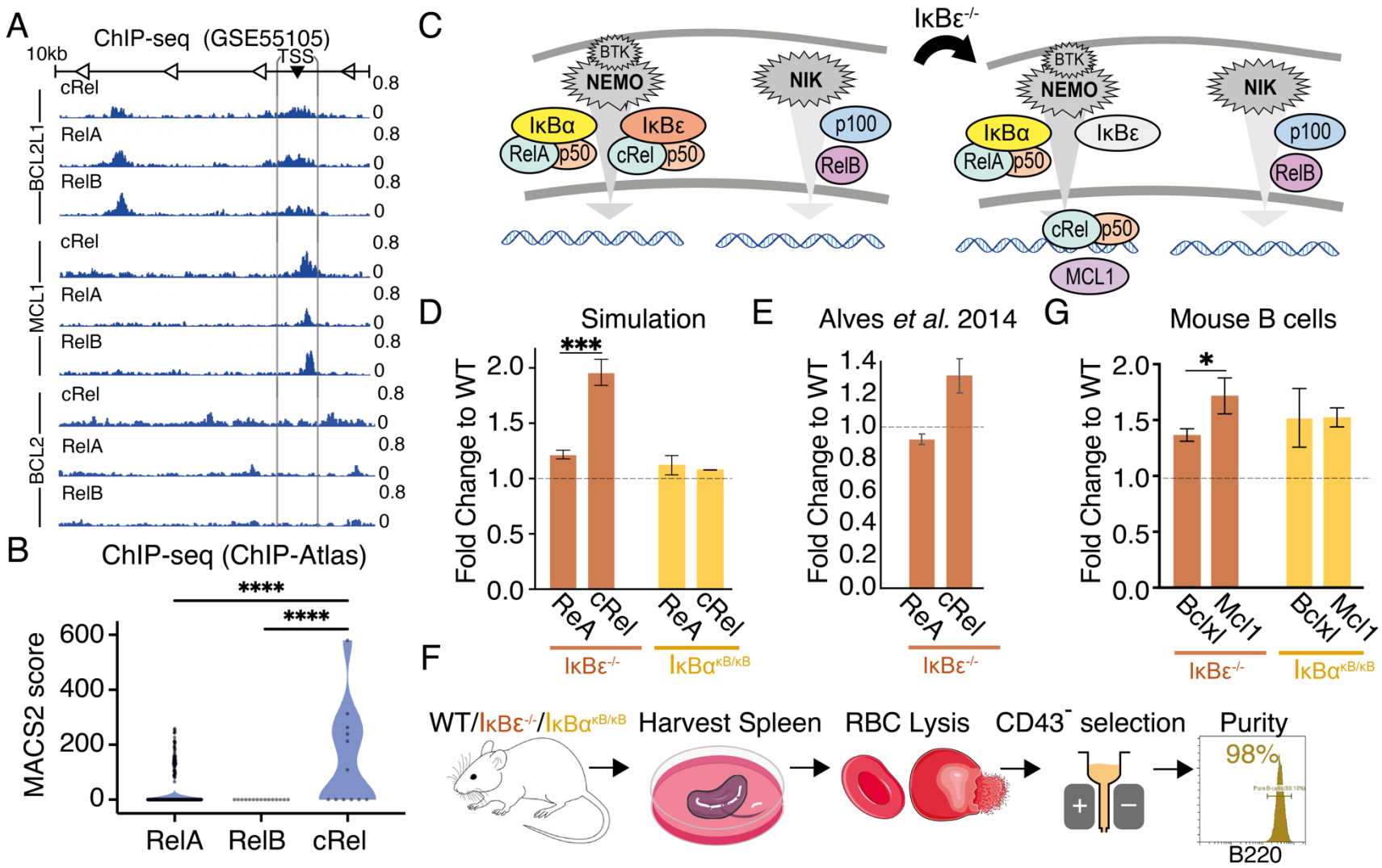
A
ChIP-seq (GSE55105)
10kb
TSS
cRel
RelA
RelB
BCL2L1
MCL1
BCL2
0.8
0
B
ChIP-seq (ChIP-Atlas)
****
****
MACS2 score
600
400
200
0
RelA
RelB
cRel
C
IκBε-/-
BTK
NEMO
NIK
IκBα
IκBε
RelA
p50
cRel
p50
p100
RelB
MCL1
D
Simulation
***
Fold Change to WT
2.0
1.5
1.0
0.5
0.0
ReA
cRel
ReA
cRel
IκBε-/-
IκBα κB/κB
E
Alves et al. 2014
Fold Change to WT
1.4
1.2
1.0
0.8
0.6
0.4
0.2
0.0
ReA
cRel
IκBε-/-
G
Mouse B cells
*
Fold Change to WT
2.0
1.5
1.0
0.5
0.0
Bclxl
Mcl1
Bclxl
Mcl1
IκBε-/-
IκBα κB/κB
F
WT/IκBε-/-/IκBα κB/κB
Harvest Spleen
RBC Lysis
CD43- selection
Purity
98%
B220

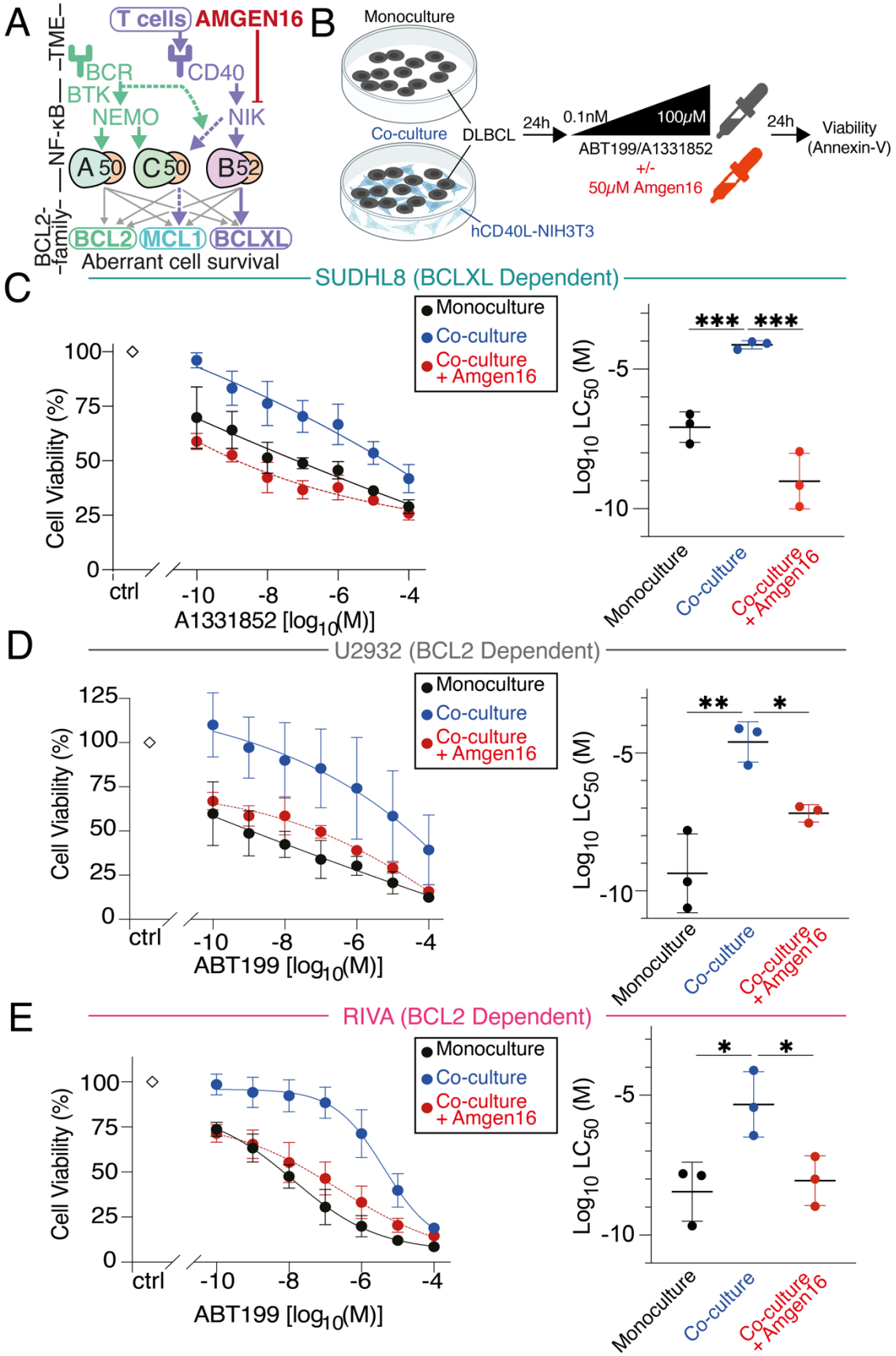
A
TME
T cells
AMGEN16
BCR
CD40
BTK
NEMO
NIK
NF-κB
A 50
C 50
B52
BCL2-family
BCL2
MCL1
BCLXL
Aberrant cell survival
B
Monoculture
Co-culture
DLBCL
hCD40L-NIH3T3
24h
0.1nM
100μM
ABT199/A1331852
+/-
50μM Amgen16
24h
Viability
(Annexin-V)
C
SUDHL8 (BCLXL Dependent)
Monoculture
Co-culture
Co-culture
+ Amgen16
Cell Viability (%)
ctrl
A1331852 [log10(M)]
Log10 LC50 (M)
***
***
D
U2932 (BCL2 Dependent)
ABT199 [log10(M)]
**
*
E
RIVA (BCL2 Dependent)
ABT199 [log10(M)]
*
*